Appl. Magn. Reson. 21, 287–297 (2001)

Applied Magnetic Resonance

© Springer-Verlag 2001
Printed in Austria

High-Field ENDOR and the Sign of the Hyperfine Coupling

B. Epel[1], P. Manikandan[1], P. M. H. Kroneck[2], and D. Goldfarb[1]

[1] Departments of Chemical Physics, Weizmann Institute of Science, Rehovot, Israel
[2] Faculty of Biology, University of Konstanz, Konstanz, Germany

Received September 26, 2001

Abstract. Two different approaches for assigning electron nuclear double resonance (ENDOR) signals to their respective M_S manifolds by a controlled generation of asymmetric ENDOR spectra, are described and applied to a number of systems. This assignment then allows a straightforward determination of the sign of the hyperfine coupling. Both approaches rely on a high thermal polarization that is easily achieved at high fields and low temperatures. For high-spin systems, such as $S = 5/2$ the assignment is afforded by the selective inversion of the $|-3/2\rangle \rightarrow |-1/2\rangle$ electron paramagnetic resonance (EPR) transition which is highly populated as compared to its symmetric counterpart, the $|1/2\rangle \rightarrow |3/2\rangle$ EPR transition, and therefore is easily identified. For $S = 1/2$ the determination of the sign of the hyperfine coupling becomes possible when the cross- and nuclear-spin relaxation rates are much slower than the electron-spin relaxation rate and variable mixing time pulse ENDOR is used to measure the spectrum. Under these conditions the signals of the $M_S = 1/2$ (α) manifold become negative when the mixing time is on order of the electron-spin relaxation time, whereas those of the $M_S = -1/2$ (β) manifold remain positive. Under partial saturation of the nuclear transitions and short mixing time the opposite behavior is observed. Pulse W-band ^{1}H ENDOR experiments demonstrating these approaches were applied and the signs of the hyperfine couplings of the water ligands in $Mn(H_2O)_6^{2+}$, the H_α and H_β histidine protons in the Cu(histidine)$_2$ complex, the imidazole protons in $Cu(imidazole)_4^{2+}$ and the cysteine β-protons in nitrous oxide reductase were determined.

1 Introduction

Electron-nuclear double resonance (ENDOR) spectroscopy is one of the most useful methods for determining the hyperfine and nuclear quadrupole interactions of nuclei in paramagnetic systems. The ENDOR spectrum provides the magnitude of the hyperfine coupling while its sign remains usually ambiguous. Relative signs of the hyperfine couplings can be determined by continuous-wave or pulse TRIPLE [1–3]. The knowledge of the sign is important for unambiguous determination of the isotropic (A_{iso}) and anisotropic parts of the interaction. Furthermore, the sign of A_{iso} is indicative of the mechanism leading to a finite spin density at the nucleus. High-field ENDOR spectroscopy, among its many other

advantages, also offers new possibilities to determine the absolute sign of hyperfine couplings. This work focuses on two such approaches; one is specific for systems with $S > 1/2$, while the other applies also to $S = 1/2$. Although the two approaches are general in terms of the nuclear spin, for simplicity we shall concentrate on ^{1}H couplings in $S = 5/2$ and $S = 1/2$ systems.

To first order, the ENDOR frequencies are given by:

$$\nu_{M_S}^{\mathrm{ENDOR}} = | M_S A - \nu_{\mathrm{H}} | , \tag{1}$$

where A is the orientation-dependent hyperfine coupling and ν_{H} is the nuclear Larmor frequency. Equation (1) is usually applicable at W-band for systems with a small zero-field splitting (ZFS). It shows that the ENDOR spectrum of an $S = 1/2$ system is symmetric about ν_{H} in the case of weak coupling ($|0.5A| < \nu_{\mathrm{H}}$) or about $0.5A$ for strong couplings ($|0.5A| > \nu_{\mathrm{H}}$), and therefore the sign of A remains unknown. Once a controlled asymmetry is introduced into the spectrum, the ENDOR lines corresponding to the different M_S manifolds can be identified and the sign of A can be determined. For a high-spin system, $S > 1/2$, this can be accomplished by measuring the ENDOR spectra in combination with a proper selection of the electron paramagnetic resonance (EPR) transitions. The presence of a small ZFS is suffice to introduce the needed separation between the various transitions to allow selective excitation. For example, for an $S = 5/2$ the selection of the $|-1/2\rangle$-$|1/2\rangle$ EPR transition generates symmetric ENDOR spectra, as in the case of $S = 1/2$, whereas selection of one of the other EPR transitions leads to ENDOR spectra that are not symmetric about ν_{H} or $0.5A$. At high fields and low temperatures the selection of the $|-5/2\rangle$-$|-3/2\rangle$ and $|-3/2\rangle$-$|-1/2\rangle$ transitions is almost automatic due to the low populations of the $|5/2\rangle$ and $|3/2\rangle$ energy levels. Consequently, the sign of the coupling can be determined from the position of the ENDOR lines with respect to ν_{H} or $0.5A$ [4, 5].

While for high-spin systems the determination of the sign of the hyperfine couplings relies on the selective excitation of specific EPR transitions, for $S = 1/2$ it takes advantage of the large thermal polarization and the spin dynamics in pulsed experiments [6, 7]. Figure 1 shows a modified version of the standard pulsed Davies ENDOR experiment [8] where an additional mixing time, t_{mix}, allowing for relaxation to take place, is introduced after the radio-frequency

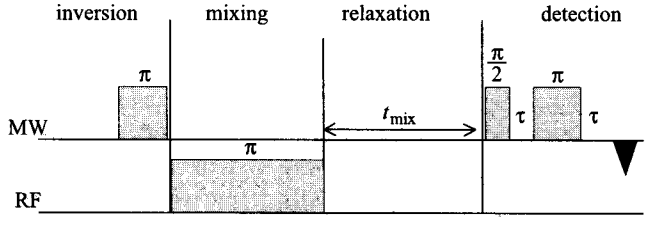

Fig. 1. Pulse sequence of the variable mixing time Davies-ENDOR experiment.

(RF) pulse and before the echo detection system [6]. In the following we shall refer to this experiment as variable mixing time ENDOR. The spectrum is obtained by measuring the echo amplitude as a function of the frequency of the RF pulse with different values of t_{mix}.

In a four-level system composed of an electron spin $S = 1/2$ coupled to one nucleus $I = 1/2$, there are three relaxation processes characterized by the electron and nuclear spin-lattice relaxation, and cross-relaxation times, T_{1e}, T_{1n}, and T_{1x} respectively, that affect the population distribution. With a general theoretical model that takes into account these relaxation processes and the thermal polarization, the ENDOR effect in the variable mixing time ENDOR experiment was calculated [7]. The ENDOR effect is defined according to:

$$F_{ENDOR} = \frac{I^{on}_{echo}(t_{mix}, t_R) - I^{off}_{echo}(t_{mix}, t_R)}{2I^0_{echo}}, \tag{2}$$

where the echo amplitudes $I^{off}_{echo}(t_{mix}, t_R)$ and $I^{on}_{echo}(t_{mix}, t_R)$ are the ENDOR signals obtained in the absence and presence of an RF pulse on-resonance with an NMR transition (in the α or β manifolds), respectively. I^0_{echo} in the denominator is the echo amplitude after a single two-pulse EPR echo experiment with the same τ as used in ENDOR experiment and $t_R \gg T_{1e}$, T_{1n}, and T_{1x}, where t_R is the repetition time. I^0_{echo} provides the normalization factor that is independent of t_R and t_{mix}. For long t_{mix}, when the spin system has relaxed to thermal equilibrium before the detection sequence, $F_{ENDOR} = 0$, whereas $F_{ENDOR} = 0.5$ when the detection sequence is applied immediately after the RF inversion pulse.

This model shows that under certain conditions the ENDOR spectrum becomes asymmetric in terms of the ENDOR effect in the α and β manifolds. The first is encountered for long mixing times, $t_{mix} \gg T_{1e}$ and T_{1n}, $T_{1x} \gg T_{1e}$, namely negligible nuclear and cross-relaxation rates. Under these conditions the ENDOR signals from the α manifold are negative and those of the β manifold positive [6]. Figure 2 depicts the dependence of $F^{\alpha,\beta}_{ENDOR}$ on t_{mix} for $T_{1n}/T_{1e} = 30$, $T_{1x} = \infty$ and for three Boltzmann factors, $h\nu/kT = 8.3$, 0.83 and 0.083. The value 0.83 corresponds to $\nu = 95$ GHz (W-band) and a temperature of 5.5 K, and the other values to 10 times higher and lower frequencies, or 10 times lower and higher temperatures. Similar results are obtained for $T_{1x}/T_{1e} = 30$, $T_{1n} = \infty$. When T_{1n} and/or T_{1x} are of the same order of t_{mix}, the absolute values of $F^{\alpha,\beta}_{ENDOR}(t_{mix})$ decrease with increasing t_{mix} and become dependent on the Boltzmann factor. The lower the temperatures, the longer it takes for the populations to reach equilibrium (for the same relaxation times).

Asymmetric ENDOR spectra can also be obtained for short t_{mix} when the cross- and/or nuclear-relaxation times are longer than the repetition time ($t_{mix} \ll T_{1e} \ll t_R$ and T_{1n}, $T_{1x} > t_R$), namely under conditions of saturations of the nuclear transitions [7]. In this case the polarization of the ENDOR signals becomes opposite to the previous case, the lines in the α manifolds are positive, while those of the β manifold are negative. Figure 3 shows the dependences of $F^{\alpha,\beta}_{ENDOR}$ on t_R. These plots also show that the optimal repetition rate for ENDOR experiments

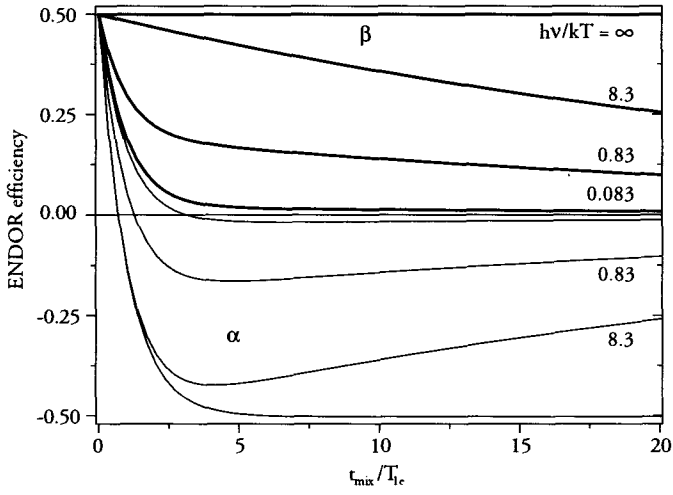

Fig. 2. Dependence of $F^{\alpha,\beta}_{ENDOR}$ on t_{mix} at different temperatures. The $h\nu/kT$ values are indicated in the figure. Thin lines correspond to F^{α}_{ENDOR} and thick lines to F^{β}_{ENDOR}. For $h\nu/kT = \infty$, $t_R = \infty$, $T_{1x} = \infty$ and $T_{1n} = \infty$. In all other cases $T_{1n}/T_{1e} = 30$, $t_R = \infty$, $T_{1x} = \infty$ [7].

which allows return to thermal equilibrium is determined by T_{1n} (or T_{1x}) and may be much longer than $5T_{1e}$.

The approach of the variable mixing time ENDOR and partial saturation of the nuclear transition is not limited to $S = 1/2$ systems. A negative ENDOR effect was observed for the ^{57}Fe W-band ENDOR line of the $M_S = -5/2$ manifold in Fe(III) substituted sodalite [4]. Although in this report the origin of the negative effect was not explained, following the model discussed above [7] it

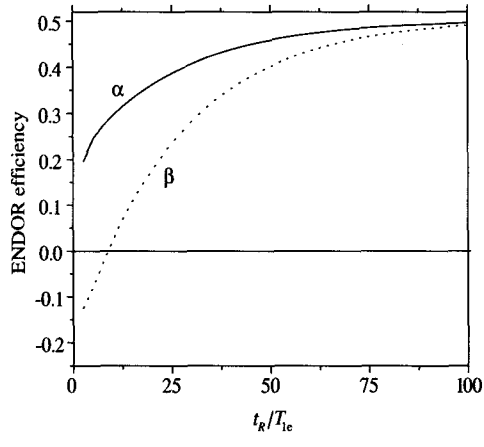

Fig. 3. Dependence of $F^{\alpha,\beta}_{ENDOR}$ on t_R for $h\nu/kT = 0.83$, $t_{mix} = 20$ μs, $T_{1x}/T_{1e} = 22$, $T_{1n} = \infty$ [7].

is clear now that the negative effect is due to a partial saturation of the nuclear transitions.

In this work we present pulsed W-band ^{1}H ENDOR measurements aimed at the determination of the absolute sign of the hyperfine couplings in a number of systems with $S = 5/2$ and $S = 1/2$ in orientationally disordered systems, employing the approaches described above. The first system concerns the coupling of water ligands in $Mn(H_2O)_6^{2+}$, the second and third involve the coupling of various ligand protons in complexes of Cu(II) with histidine (CuHis) and imidazole (CuImid), and the fourth concentrates on the strongly coupled cysteine β-protons in the mixed valent, binuclear Cu_A center of nitrous oxide reductase (N_2OR).

2 Experimental

2.1 Sample Preparation

The $Mn(H_2O)_6^{2+}$ solution was prepared by dissolving $MnCl_2$ in a 50/50 water-glycerol solution with a final concentration of 1 mM. The Cu(histidine)$_2$ complex (CuHis) in D_2O was prepared according to reported procedures [9]. A typical preparation procedure involves mixing, in a molar ratio of 1:5, anhydrous $CuCl_2$ and L-histidine · HCl · H_2O in D_2O (Cambridge Isotope Laboratories, Inc.). The solution was stirred for an hour at room temperature. The pD of the solution was adjusted to 7.3 with 0.1 N NaOD (ISOTEC, Inc.) and/or dilute D_2SO_4 (Sigma Co.) solutions. Glycerol-d_3 (Cambridge Isotope Laboratories, Inc.) was used to produce a good glass upon freezing. The [Cu(imidazole)$_4$]Cl_2 complex (CuImid) was prepared also in a 50/50 water-glycerol solution, as reported earlier [10]. The concentration of the Cu(II) complexes was 2 mM. All the chemicals were used without further purifications. Nitrous oxide reductase samples, from *Pseudomonas stutzeri*, was prepared as described in ref. 11.

2.2 Spectroscopic Measurements

All measurements were performed at W-band (94.9 GHz) on a homebuilt spectrometer [12] at 4–5 K. Field-sweep echo-detected (FS-ED) EPR spectra were recorded with the two-pulse echo sequence, with microwave (MW) $\pi/2$ and π pulses of 0.05 and 0.1 μs, respectively, and $\tau = 0.25$–0.3 μs. In this experiment the echo amplitude is measured as a function of the magnetic field. The magnetic field values were calibrated according to the Larmor frequency of the protons, ν_H, obtained from ENDOR spectra. The ENDOR measurements were carried out with microwave $\pi/2$ and π pulses of 0.1 and 0.2 μs, respectively, and with an echo delay time, τ, of 0.35–0.5 μs. The RF pulse length, t_{RF}, was in the range of 14–25 μs. Unless stated otherwise $t_{mix} = 2$–4 μs and the repetition rate, t_R, was 10 ms. The frequency scale in ENDOR spectra is given with respect to the Larmor frequency, $\nu = \nu_{RF} - \nu_H$.

3 Results and Discussion

3.1 $Mn(H_2O)_6^{2+}$

The FS-ED EPR spectrum of a frozen solution of $Mn(H_2O)_6^{2+}$ is shown in the inset of Fig. 4. It consists of a well resolved sextet superimposed on a broad asymmetric background with a total width of about 1000 G. The six narrow peaks correspond to the ^{55}Mn ($I = 5/2$) hyperfine components of the $|-1/2, m\rangle \rightarrow |1/2, m\rangle$ EPR transitions centered at $g = 2$. The background is due to a superposition of the powder patterns of all other EPR transitions with integrated intensities in the following order: $|-5/2, m\rangle \rightarrow |-3/2, m\rangle > |-3/2, m\rangle \rightarrow |-1/2, m\rangle > |1/2, m\rangle \rightarrow |3/2, m\rangle > |3/2, m\rangle \rightarrow |5/2, m\rangle$ due to the thermal polarization. The ^1H ENDOR spectrum, recorded at the field position denoted by A (bottom trace, Fig. 4) consists of a superposition of two "Pake" doublets. The inner one, with a splitting of about 1 MHz corresponds to distant solvent protons, whereas the second, with $A_\perp$ and $A_\parallel$ singularities at ± 1.25 and ± 3.67 MHz, is due to the water ligands. The rather symmetric appearance of this spectrum indicates that it originates primarily from a $|-1/2, m\rangle \rightarrow |1/2, m\rangle$ EPR transition. However, considering the FS-ED spectrum and the field at which the spectra were measured, contributions from the $|-5/2, m\rangle \rightarrow |-3/2, m\rangle$ and $|-3/2, m\rangle \rightarrow |-1/2, m\rangle$ EPR transitions are expected as well. A close look at the low-frequency end of the spectrum indeed reveals a signal from the $M_S = -3/2$ manifold superimposed on the $A_\parallel$ feature of the $M_S = 1/2$. The ENDOR spectrum recorded at positions B, outside the range of the $|-1/2, m\rangle \rightarrow |1/2, m\rangle$ EPR transitions (top trace, Fig. 4), where the major contributions to the spectrum come from the $|-3/2, m\rangle \rightarrow |-1/2,$

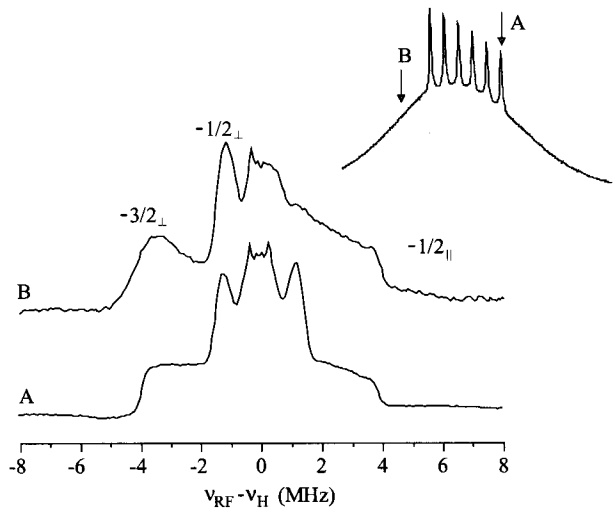

Fig. 4. ^1H ENDOR spectra of $Mn(H_2O)_6^{2+}$ (4.5 K, $t_{RF} = 15$ μs, $t_R = 10$ ms) measured at two different field positions, A and B, as indicated in the inset which shows the FS-ED EPR spectrum.

$m\rangle$ transition is significantly different. It clearly shows the $A_{\|}$ and $A_{\perp}$ features of the $M_S = -1/2$ manifold, along with the $A_{\perp}$ singularity of the $M_S = -3/2$ manifold. The powder pattern of the $M_S = 1/2$ manifold has completely disappeared. From this spectrum we determined that $A_{\|} > 0$ and $A_{\perp} < 0$ as expected for a hyperfine interaction dominated by a dipolar contribution. With these two values we obtained a positive small isotropic coupling, $A_{iso} = 0.39$ MHz in agreement with the values obtained earlier from X-band measurements [13].

3.2 Cu(histidine)$_2$

The FS-ED EPR spectrum of CuHis prepared in D_2O is shown in the inset of Fig. 5 and ^{1}H ENDOR spectra were measured at the $g_{\perp}$ and $g_{\|}$ positions. The ENDOR spectrum recorded at $g_{\perp}$ (bottom trace, Fig. 5) consists of a doublet at ± 5.2 MHz, assigned to the H_α protons, and two powder patterns in the center of the spectrum. The powder pattern at ± 1.09 and ± 2.0 MHz is assigned to imidazole protons, whereas the singularities at ± 0.62 MHz are due to the H_β protons [5]. While at $g_{\perp}$ the ENDOR spectrum is rather symmetric with respect to ν_H, the spectrum recorded at $g_{\|}$ is highly asymmetric as shown in the top trace of Fig. 5. In this spectrum the high-frequency component of the H_α protons has completely vanished and the central powder pattern is dominated by a strong peak at 0.6 MHz. Since these spectra were recorded with t_{mix} of 2 μs, which is considerably shorter than T_{1e}, we attribute the asymmetry to a partial saturation of the nuclear transitions. Under these conditions the disappearing signal corresponds to the β-manifold (see Fig. 3), yielding a positive hyperfine coupling (see Eq. (1)). Moreover, the two ENDOR spectra show that the hyperfine coupling of the H_α protons is primarily isotropic and therefore $A_{iso} > 0$. The intense feature in the central powder pattern is due to the H_β protons experiencing a negative coupling.

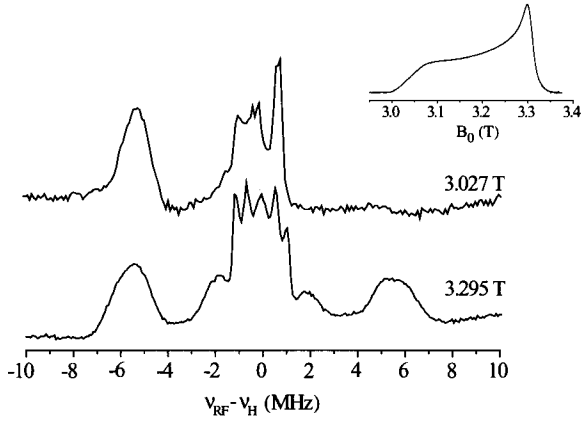

Fig. 5. ^{1}H ENDOR spectra of the CuHis complex in D_2O measured at $g_{\|}$ ($B_0 = 3.027$ T) and $g_{\perp}$ ($B_0 = 3.295$ T) (4.5 K, $t_{RF} = 25$ μs, $t_R = 10$ ms). The inset shows the FS-ED EPR spectrum.

The observed asymmetry in the ENDOR spectrum recorded at the $g_{\|}$ position and its absence in the spectrum recorded in the $g_{\perp}$ indicate that at $g_{\|}$ T_{1x}/T_{1e} is much larger than at $g_{\perp}$, assuming that in both cases T_{1n} is very long and can be neglected.

3.3 Cu(imidazole)$_4^{2+}$

The FS-ED EPR spectrum of CuImid is similar to that of CuHis, and as in CuHis asymmetric spectra are observed at $g_{\|}$, whereas at $g_{\perp}$ the spectra are reasonably symmetric. Variable mixing time ENDOR spectra recorded at $g_{\|}$ are shown in Fig. 6. A symmetric spectrum, with two broad doublets at ± 2 and ± 0.5 MHz, is observed for $t_{mix} = 986$ μs. Comparison with the ENDOR spectrum recorded at $g_{\perp}$ (not shown) shows that the ± 2 MHz doublet corresponds to the A_{zz} features of the two protons that are the closest to the bound nitrogen [5]. The t_{mix}

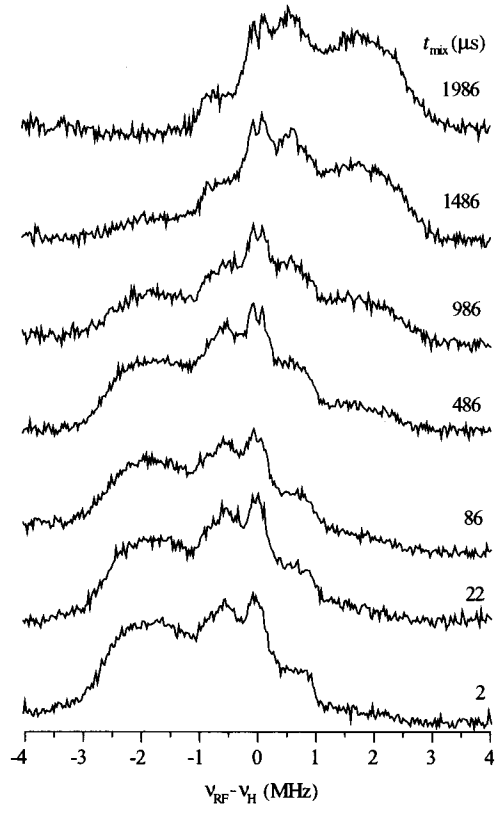

Fig. 6. ^{1}H ENDOR spectra of the CuImid complex measured at $g_{\|}$ (3.020 T), (4.5 K, $t_{RF} = 14$ μs, $t_R = 8$ ms) with different t_{mix} values as listed in the figure.

dependence of the spectrum is typical for spectra recorded under partial saturation of the nuclear transitions [7]. At short mixing times, the intensity of the 2 MHz peak is close to zero, identifying it as belonging to the β-manifold which yields $A_{zz} > 0$ (see Fig. 3). As t_{mix} increases, the intensity of the 2 MHz signal increases, whereas that of the −2 MHz decreases and finally becomes negative, thus reaching the conditions of a negative ENDOR effect for the α-manifold, again consistent with $A_{zz} > 0$.

3.4 N_2OR

At the resting, oxidized state N_2OR contains one EPR active center, the electron transfer-mediating Cu_A center. It is a mixed valent, binuclear copper center with total of one unpaired electron ($S = 1/2$), which is highly delocalized with each copper having a formal oxidation state of 1.5 [14]. The two coppers are bridged by two thiolates from two cysteines and are each further coordinated to a histidine and a weak axial ligand, a methionine and a main chain carbonyl of a tryptophan [15]. One of the unique spectroscopic features of the Cu_A site is the high A_{iso} of the cysteine β-protons arising from the large spin density on the thiolates [16]. The isotropic hyperfine coupling of these protons contains important spatial and electronic structural information because it is related to the HCSS dihedral angle, ϕ, according to [16]:

$$A_{iso} = \rho_S (B \sin^2 \phi + C), \tag{3}$$

where ρ_S is the sulfur spin density, B represents the part of A_{iso} that results from hyperconjugation and is orientation-dependent, whereas C is a measure of the contribution of other mechanism such as spin polarization. The A_{iso} values can be determined from simulations of a series of orientation-selective ENDOR spectra that allows the separation of the isotropic and anisotropic parts of the interaction. Such simulations, however, are often not unique and yield two sets of parameters, one with positive and the other with negative values of A_{iso}, which fit equally well the experimental spectra. Therefore, an independent determination of the sign of the couplings is essential for obtaining accurate A_{iso} values from which $\rho_S B$ and $\rho_S C$ can be obtained and conclusions regarding the spin density distribution in the site can be drawn. In the following we show that the sign of A_{iso} of the cysteine β-protons can be determined from variable mixing time ENDOR measurements carried out at the $g_{||}$ position.

The FS-ED EPR spectrum of N_2OR is presented in the inset of Fig. 7. It shows that in addition to the Cu_A center ($g_{xx} = 2.005$, $g_{yy} = 2.02$, $g_{zz} = 2.175$), minor amounts of a normal Cu(II), with $g_{\perp} = 2.04$ (of about 3.3 T), are present as well. The latter does not interfere with the ENDOR measurements as it does not have ENDOR signals in the region of the β-protons. ^{1}H ENDOR spectra of N_2OR, recorded at the g_{zz} position with a short t_{mix} is shown at the top of Fig. 7. Two types of protons are recognized. The first consists of protons with large,

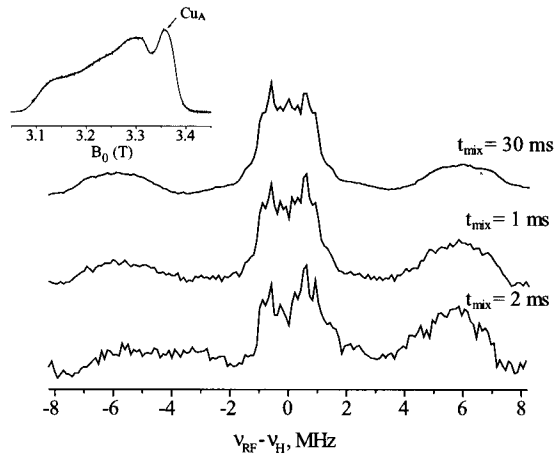

Fig. 7. ^{1}H W-band ENDOR spectra of a frozen solution of N_2OR recorded at 4.5 K and 3.128 T ($g_{||}$ position) and measured with various values of t_{mix} as listed in the figure (t_{RF} = 25 μs, t_R = 20 ms).

mostly isotropic hyperfine couplings in the range of 9–14 MHz attributed to the cysteine β-protons [16, 17], whereas the second comprises the weakly coupled protons with couplings smaller than 3 MHz that arise from other protons in the site. Spectra recorded at other fields have the same general features, though the detailed line-shapes are different, exhibiting a better resolution within the β-protons doublets. Spectra measured with longer mixing times (see Fig. 7) show a significant reduction in the intensity of the low-frequency component of the doublet, assigning it to the α-manifold, yielding positive hyperfine couplings and positive A_{iso} values. The positive paramagnetic shifts of cysteine β-protons observed in the NMR spectra of other Cu_A sites are consistent with this assignment [18, 19].

4 Conclusions

Pulsed ENDOR measurements carried out under large thermal polarization, namely, high fields and low temperatures, often allow a straightforward determination of the sign of the hyperfine coupling. For $S = 5/2$ this is afforded by the selection of the $|-3/2\rangle \rightarrow |-1/2\rangle$ EPR transition which is highly populated as compared to its symmetric counterpart, the $|1/2\rangle \rightarrow |3/2\rangle$ EPR transition. For $S = 1/2$ the determination of the sign of the hyperfine becomes possible when the cross and nuclear-spin relaxation rates are much slower than the electron-spin relaxation rates and measurements are carried out with variable mixing time ENDOR. Under these conditions the ENDOR spectrum becomes asymmetric when t_{mix} is on order of T_{1e}, or when measurements are carried out under partial saturation of the nuclear transitions and t_{mix}.

These approaches were applied to: (i) $Mn(H_2O)_6^{2+}$ where for the water ligands $A_\perp < 0$ and $A_\parallel > 0$, (ii) the Hα histidine protons in the $Cu(histidine)_2$ complex for which $A_{iso} > 0$, and the β-proton with $A_\perp < 0$, (iii) the imidazole protons in $Cu(imidazole)_4^{2+}$ where $A_\parallel > 0$ and (iv) the cysteine β-protons in N_2OR for which $A_{iso} > 0$.

Acknowledgements

This work was supported by the DFG Schwerpunkt program "High-Field EPR in Physics, Chemistry and Biology" and by the German-Israel Foundation for Scientific Research.

References

1. Cook R.J., Whiffen D.H.: Proc. Phys. Soc. **84**, 845–848 (1964)
2. Biehl B., Plato M., Möbius K.: J. Chem. Phys. **63**, 3515–3522 (1975)
3. Mehring M., Höfer P., Grupp. A.: Ber. Bunseges. Phys. Chem. **91**, 1132–1137 (1987)
4. Goldfarb D., Strohmaier K.G., Vaughan D.E.W., Thomann H., Poluektov O., Schmidt J.: J. Am. Chem. Soc. **118**, 4665–4671 (1996)
5. Manikandan P., Epel B., Goldfarb D.: Inorg. Chem. **40**, 781–787 (2001)
6. Bennebroek M.T., Schmidt J.: J. Magn. Reson. **128**, 199–206 (1997)
7. Epel B., Poppl A., Manikandan P., Vega S., Goldfarb D.: J. Magn. Reson. **148**, 388–397 (2001)
8. Davies E.R.: Phys. Lett. A **47**, 1 (1974)
9. Sigel H., Griesser R., McCormick D.B.: Arch. Biochem. Biophys. **134**, 217–227 (1960)
10. Van Camp H., Sands R.H., Fee J.A.: Biochim. Biophys. Acta. **704**, 75–89 (1982)
11. Alvarez M.L., Ai J., Zumft W., Sanders-Loehr J., Dooley D.M.: J. Am. Chem. Soc. **123**, 576–587 (2001)
12. Gromov I., Krymov V., Manikandan P., Arieli D., Goldfarb D.: J. Magn. Reson. **139**, 8–17 (1999)
13. Tan X., Bernardo M., Thomann H., Scholes C.P.: J. Chem. Phys. **98**, 5147–5157 (1993)
14. Kroneck P.M.H. in: Handbook of Metalloproteins (Messerscmidt A., Huber R., Poulos T., Wieghart K., eds.), vol. 2, pp. 1133–1341. New York: John Wiley 2000.
15. Brown K., Tegoni M., Prudencio M., Pereira A.S., Besson S., Moura J.J., Moura I., Cambillau C.: Nat. Struct. Biol. **7**, 191–195 (2000)
16. Neese F., Kappl R., Hutterman J., Zumft W.G., Kroneck P.M.H.: J. Bioinorg. Chem. **3**, 53–67 (1998)
17. Slutter C.E., Gromov I., Epel B., Richards J.H., Pecht I., Goldfarb D.: J. Am. Chem. Soc. **123**, 5325–5336 (2001)
18. Salgado J., Warmerdam G., Bubacco L., Canters G.W.: Biochemistry **37**, 7378–7389 (1998)
19. Luchinat C., Soriano A., Djinovic-Carugo K., Saraste M., Malmstrom B.G., Bertini I.: J. Am. Chem. Soc. **119**, 11023–11027 (1997)

Authors' address: Daniella Goldfarb, Department of Chemical Physics, Weizmann Institute of Science, Rehovot 76100, Israel
E-mail: daniella.goldfarb@weizmann.ac.il